

Local Mechanism Governs Global Reinforcement of Nanofiller-Hydrogel Composites

Ippolyti Dellatolas,^{*,#} Minaspi Bantawa,[#] Brian Damerou, Ming Guo, Thibaut Divoux, Emanuela Del Gado, and Irmgard Bischofberger^{*}



Cite This: <https://doi.org/10.1021/acsnano.3c00716>



Read Online

ACCESS |



Metrics & More



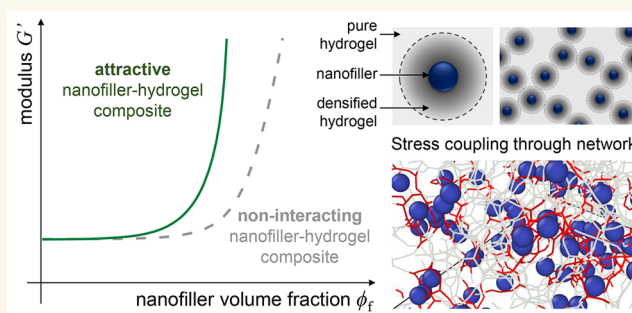
Article Recommendations



Supporting Information

ABSTRACT: We reveal the mechanism for the strong reinforcement of attractive nanofiller-hydrogel composites. Measuring the linear viscoelastic properties of hydrogels containing filler nanoparticles, we show that a significant increase of the modulus can be achieved at unexpectedly low volume fractions of nanofillers when the filler-hydrogel interactions are attractive. Using three-dimensional numerical simulations, we identify a general microscopic mechanism for the reinforcement, common to hydrogel matrices of different compositions and concentrations and containing nanofillers of varying sizes. The attractive interactions induce a local increase in the gel density around the nanofillers. The effective fillers, composed of the nanofillers and the densified regions around them, assemble into a percolated network, which constrains the gel displacement and enhances the stress coupling throughout the system. A global reinforcement of the composite is induced as the stresses become strongly coupled. This physical mechanism of reinforcement, which relies only on attractive filler-matrix interactions, provides design strategies for versatile composites that combine low nanofiller fractions with an enhanced mechanical strength.

KEYWORDS: nanofillers, hydrogel composites, reinforcement, stress coupling, hydrogel densification



Hydrogels consist of a sparse network embedded in water. Their high water content makes these materials versatile in food science, cosmetics and bioengineering,^{1–6} yet low elasticity and weak mechanical properties can limit their scope.⁷ Recent efforts have expanded the range of material performance and applications beyond those previously considered possible.⁸ For example, adding transient bonds to a permanently cross-linked gel matrix can help achieve higher extensibility,⁹ or intertwining two polymer networks, one highly and the other loosely cross-linked, leads to materials with superior fracture toughness.^{10,11} Using inorganic nanofillers has been shown to enhance both toughness and extensibility in polymer-clay nanocomposites, where clay platelets act as multifunctional dynamical cross-links.¹² However, these effects depend unpredictably on the size and surface properties of the nanofillers, as well as on the chemistry of the polymer matrix.¹³ Moreover, ensuring that the nanofillers act as multifunctional cross-links often requires precise engineering of their surface chemistry, specific to the polymer matrix used,^{13–17} which limits this method's versatility. If there were general, system-independent mecha-

nisms for reinforcing hydrogels through the addition of nanofillers, one could fabricate materials that combine exceptional mechanical performance and functionalization through properties conferred by the nanofillers. Here, we make a significant step toward this goal.

Studies in other soft materials suggest that the nanofiller-induced changes in the composite structure, dynamics, and mechanical response are sensitively dependent on the nature of the interactions between the fillers and the matrix. Attractive nanofillers can significantly reduce the mobility of a surrounding polymer melt matrix,^{18–21} or increase the entanglements in elastomers²² and entangled polymers.^{23,24} In block copolymers and microemulsion gels, adding attractive

Received: January 24, 2023

Revised: October 16, 2023

Accepted: October 18, 2023

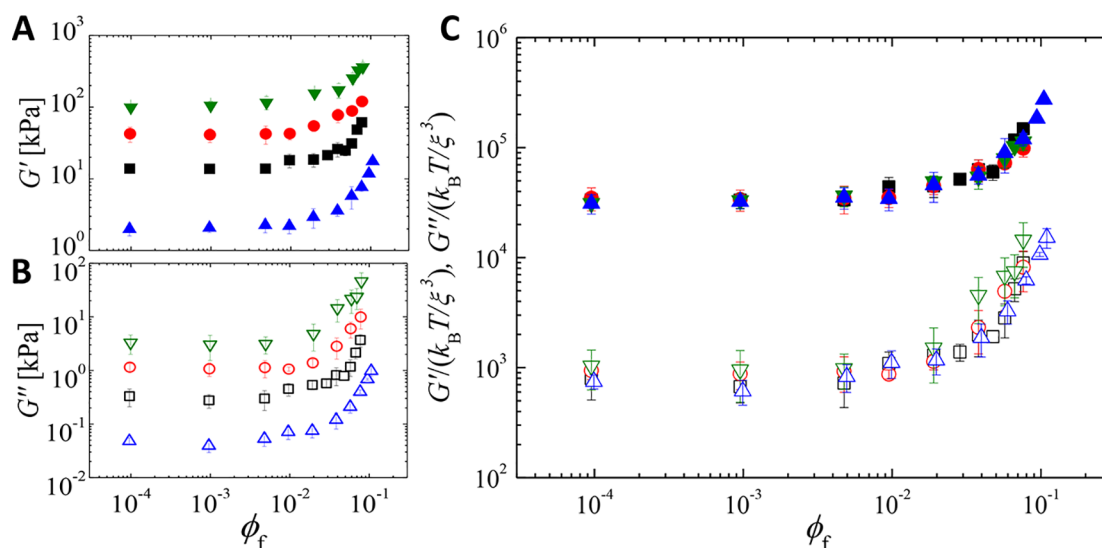


Figure 1. Reinforcement of agarose gels by polystyrene nanofillers. (A) Storage modulus G' and (B) loss modulus G'' of the filler-hydrogel composites versus filler volume fraction ϕ_f . Polystyrene particles of radius $r_f = 100$ nm are embedded in agarose gels of concentration 0.5 wt % (\blacktriangle), 1 wt % (\blacksquare), 2 wt % (\bullet), and 4 wt % (\blacktriangledown). (C) Storage and loss moduli normalized by the entropic modulus $k_B T/\xi^3$, where ξ is the mesh size of the agarose gels measured by particle tracking in confocal microscopy in the absence of nanofillers. The normalized G' and G'' for the four agarose concentrations collapse onto master curves.

nanofillers can lead to reinforcement by locally altering the matrix structure.^{25–28} In soft biological tissues, the presence of nanofillers or cells that adhere to the fibrous extracellular matrix affects the stiffening or softening under tension or compression.^{29,30} In hydrogels, the elastic properties have been shown to increase at nanofiller volume fraction of about 50% for repulsive filler–matrix interactions.^{31–34} The reinforcement is then well-described by the Guth–Gold model, which generalizes Einstein’s equation for the composite modulus to account for filler–filler interactions,³⁵ and by effective medium formulations,³⁶ including a Krieger–Dougherty-like equation for the storage modulus.³⁷ For attractive filler-hydrogel interactions, by contrast, the increase of the storage modulus has been reported at significantly lower nanofiller volume fractions and to be stronger than that predicted by these models; however, a physical mechanism for the reinforcement has not been proposed.^{38,39}

Here, we demonstrate that attraction between the nanofillers and the hydrogel is indeed essential for reaching a strong reinforcement in composite materials at a low volume fraction of nanofillers. Using a combination of experiments and simulations, we propose a general physical mechanism for reinforcement of the composite elasticity in attractive filler-gel systems. The filler–matrix attraction leads to a densification of the gel matrix around the nanofillers. The new unit of “effective filler”, comprised of the nanofillers and their densified shells, percolates through the matrix, enhancing long-range stress correlations at relatively low nanofiller volume fractions. As a result, the microscopic fluctuations of the gel become significantly reduced, leading to the reinforcement of the composite’s macroscopic elastic properties.

RESULTS AND DISCUSSION

Reinforcement of Attractive Nanofiller-Hydrogel Composites. We probe the mechanical properties of agarose gels with embedded carboxylated polystyrene nanofillers of radius $r_f = 100$ nm. The nanofillers physically bind to the agarose gel matrix through hydrogen bonding.⁴⁰ Adding fillers

at volume fraction $\phi_f \lesssim 0.01$ does not modify the linear viscoelastic properties of the agarose gel. For $\phi_f \gtrsim 0.01$, however, both the storage modulus G' and the loss modulus G'' increase strongly with increasing nanofiller content within a small range of nanofiller volume fractions; a 10-fold increase of both moduli is reached at $\phi_f \approx 0.10$, as shown in Figures 1A and B. This reinforcement of the moduli is systematically observed for agarose concentrations ranging from 0.5 wt % to 4 wt %. Both $G'(\phi_f)$ and $G''(\phi_f)$ can be rescaled onto master curves by normalizing the moduli with the entropic modulus $k_B T/\xi^3$, as shown in Figure 1C, where k_B is the Boltzmann constant, T the temperature, and ξ the mesh size of the agarose gel (see Table S1 in the Supporting Information). The agarose concentrations are chosen such that the mesh size of the gel is slightly larger than the nanofiller diameter $2r_f$ for the lowest agarose concentration and smaller than $2r_f$ for the highest agarose concentration, which suggests that the reinforcement is not governed by the confinement of the nanofillers in the polymer network characterized by the ratio of the gel mesh size to the nanofiller diameter $\xi/2r_f$. To confirm this observation, we vary the filler radius from $r_f = 100$ nm to $r_f = 500$ nm for a fixed agarose concentration of 0.5 wt %; indeed, the storage modulus normalized by the modulus of the pure agarose gel, G'/G_0 , exhibits an identical reinforcement for all nanofiller sizes, as shown in Figure 2A. The reinforcement is thus controlled by the volume occupied by the nanofillers rather than by the filler surface area or the number of fillers.

To investigate whether the observed reinforcement arises from a mechanism specific to the agarose-filler composite, we use another physical biopolymer matrix, gelatin,⁴⁰ and a chemical synthetic hydrogel matrix, polyacrylamide,⁴¹ with which the polystyrene nanofillers exhibit attractive electrostatic interactions.^{42–45} In both cases, we find a similar reinforcement upon the addition of nanofillers, with only a weak dependence on the nature of the hydrogel matrix, as shown in Figure 2A. Confocal microscopy and small-angle X-ray scattering experiments show that the nanofillers are well dispersed in the hydrogel, demonstrating that the reinforce-

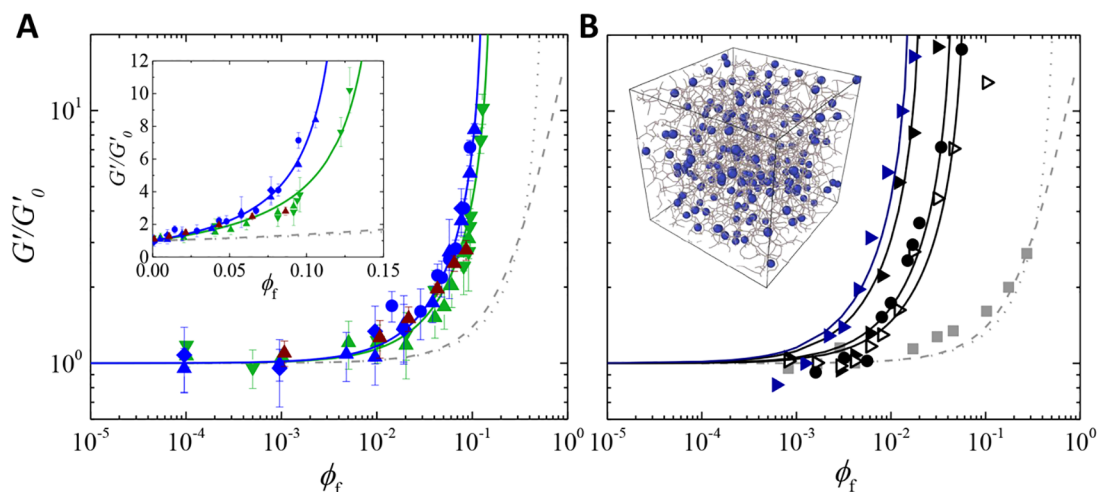


Figure 2. Generic reinforcement in attractive filler-hydrogel systems. (A) Reinforcement of the normalized storage modulus G'/G'_0 of agarose (blue), gelatin (green), and polyacrylamide (wine) hydrogels by polystyrene nanofillers of radius $r_f = 20$ nm (\blacktriangledown), 100 nm (\blacktriangle), 250 nm (\bullet), and 500 nm (\blacklozenge). (B) Reinforcement obtained in simulations for attractive filler-gel systems of attraction strength 1ϵ in a gel of concentration $\phi_{\text{gel}} = 0.10$ containing nanofillers of diameter $d_f = 1.6d$ (black, \blacktriangleright), in $\phi_{\text{gel}} = 0.1$ containing fillers of $d_f = 2d$ (black, \bullet), in $\phi_{\text{gel}} = 0.1$ containing nanofillers of $d_f = 1.6d$ (open, \blacktriangleright), and for repulsive filler-gel systems in a gel of concentration $\phi_{\text{gel}} = 0.10$ containing nanofillers of $d_f = 1.6d$ (gray, \blacksquare). ϵ is the unit energy in the simulations corresponding to the attraction strength between gel particles in the network (see the [Numerical Methods](#)). Inset: Snapshot of the simulation for $\phi_f = 0.017$. The blue spheres represent the nanofillers; the gray segments denote the gel network. The reinforcement of all of the attractive systems is stronger than that predicted by the Guth–Gold model (dashed line) and the Krieger–Dougherty model (dotted line). A two-step reinforcement model describes the strong reinforcement (solid lines); details of the model and fit parameters are given in the [Supporting Information](#). G'_0 denotes the storage modulus of the gel without nanofillers.

ment is not due to the aggregation of the nanofillers in the composites (see [Supporting Information](#)).

The robustness of our experimental results points toward a general reinforcement mechanism with a common microscopic origin. To access the changes in the microscopic structure and dynamics of the gel network induced by the nanofillers and to probe the role of the filler–matrix attraction for the reinforcement, we perform three-dimensional molecular dynamics (MD) simulations of spherical nanofiller particles embedded in a model coarse-grained gel matrix composed of gel particles (see [Numerical Methods](#)). For attractive filler-gel systems, the simulations confirm the strong increase in the storage modulus at a low nanofiller volume fraction observed in the experiments. The functional form of the reinforcement remains similar over a range of nanofiller sizes, gel concentrations, and polymer–filler attraction strengths, in agreement with the experimental results. The strength of reinforcement increases with increasing attraction strength, while it decreases slightly with increasing polymer concentration and increasing nanofiller size, as shown in [Figure 2B](#). In all attractive systems in both experiments and simulations, the reinforcement is much stronger than the one predicted by the Guth–Gold model, which adapts Einstein’s equation for the volume fraction dependence of the viscosity of hard-sphere suspensions to describe the modulus of composite gels accounting for filler–filler interactions,³⁵ and by an effective-medium formulation of the Krieger–Dougherty equation,³⁷ as shown by the dashed lines in [Figure 2](#). For repulsive filler-gel systems, in contrast, the composite gel exhibits a reinforcement occurring at larger nanofiller volume fractions that is well-described by the Guth–Gold model and by the extension of Krieger–Dougherty’s equation to gels ([Figure 2B](#)). Importantly, neither the attractive filler-gel systems in the MD simulations nor the experimental results can be described by

these models. These findings not only confirm that the attractive interactions between the nanofillers and the gel matrix are key for the low volume fraction reinforcement observed here but also strongly suggest that the attraction changes the nature of the reinforcement mechanism.

Local Gel Density and Characterization of Densified Shell. To probe the changes induced by the nanofillers in the hydrogel matrix, we measure the local gel density around each nanofiller of radius r_f in layers of thickness ΔR varying between $0.8r_f$ and $1.6r_f$ in simulations. When the filler-gel interactions are attractive, we observe a densification of the gel around the nanofiller, characterized by a region that we denote as “shell” where the density is higher than the average gel density, as shown in [Figure 3](#). The maximum thickness ΔR_{max} beyond which the gel density approaches that of the average gel density, provides an estimate of the shell thickness δ , which we find to be $\delta \sim 1.4r_f$. The shell forms at any nanofiller volume fraction, including at nanofiller fractions below the onset of reinforcement, and its thickness is independent of ϕ_f ([Figure 3B](#)). For repulsive filler–matrix interactions, however, such densification does not occur, and we observe a slight depletion of the gel close to the nanofillers. These findings confirm that in the attractive composites the nanofillers induce a local change in the hydrogel matrix at low nanofiller volume fractions. In the experiments, the attractive interactions between the nanofillers and the hydrogel matrix are likewise expected to lead to an increased number density of polymer chains close to the nanofillers. Combined with gelation, the formation of a bound layer of polymer around the nanofillers then leads to a local increase of the hydrogel density. Strong reinforcement is observed for nanofillers whose radius is larger than or comparable to the gel mesh size. Below a certain ratio of nanofiller radius to gel mesh size, we do not observe strong reinforcement, suggesting that as the nanofillers become too

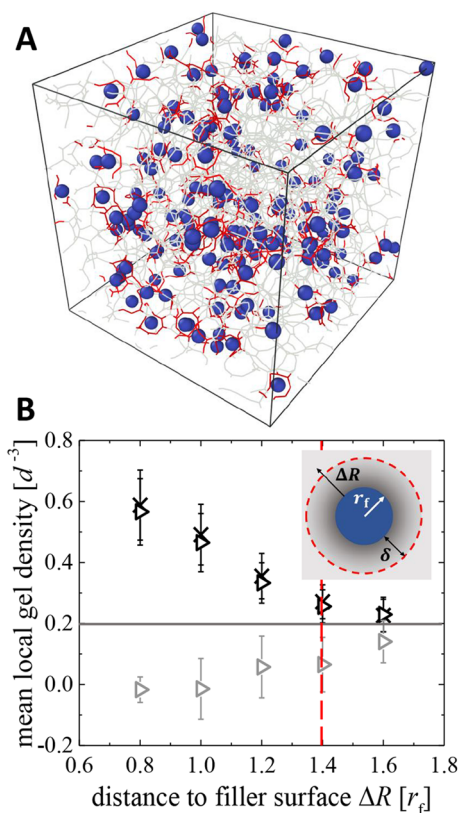


Figure 3. Local densification of the gel network around the nanofillers in attractive filler-gel systems. (A) The simulation snapshot indicates the regions where the gel density is higher than the average density (red segments), regions of average gel density (gray segments), and nanofillers (blue) for the attractive filler-gel system of attraction strength 1ϵ . (B) For the attractive filler-gel systems, the local gel density decreases with distance to the nanofiller surface ΔR . The variation in gel density with distance to nanofiller surface is similar for gels containing nanofillers at a volume fraction higher than the onset of reinforcement, $\phi_f = 0.017$ (black, \triangleright), and for gels with a volume fraction of nanofillers lower than the onset of reinforcement, $\phi_f = 0.00164$ (black, \times). For repulsive filler-gel systems at $\phi_f = 0.017$, there is no densification close to the nanofillers where the local gel density is lower than the average gel density (gray, \triangleright). The solid gray line denotes the average gel density. The dashed red line indicates the estimated shell thickness, δ , determined as the region with gel density higher than the average density.

small compared to the mesh size, they can no longer induce local densification. In a different class of composite materials exhibiting attractive filler–matrix interactions, in filler-reinforced rubbers, an interphase of stiffer elastomers has been shown to form around nanofillers. The reinforcement in the filler-reinforced rubbers was successfully described by an effective medium model that accounts for this stiffer region.⁴⁶ Such a model accurately captures the reinforcement of our soft hydrogel composites, in both experiments and simulations, as shown in Figure 2. Details of the model and its relation to other effective medium theories³⁶ are provided in the Supporting Information. The reinforcement is also well described by a modification of the Guth–Gold equation using an effective filler volume fraction to account for the presence of a shell, as shown in the Supporting Information. The MD simulations allow us to probe the impact of the effective fillers at the microscopic level and to address how the

local modification to the gel structure induced by the nanofillers leads to the global strengthening of the composite material.

Percolation of Effective Fillers and Stress Coupling Throughout the Composite Material.

With increasing nanofiller volume fraction, the effective fillers occupy an increasingly larger fraction of the composite material. We hypothesize that the onset of the reinforcement is related to the percolation of effective fillers into a space-spanning network, which alters the microscopic dynamics and mechanical properties of the composite. To compute the probability for a percolating network of effective fillers to form, we first consider any two effective fillers to be part of the percolating structure if the distance between their centers is equal to or less than a connectivity distance l (see inset in Figure 4B). We then determine the percolation probability \mathbb{P} from the occurrence of a percolating network of effective fillers for 60 independently generated samples. We measure \mathbb{P} for different connectivity distances l for various nanofiller volume fractions (Figure 4A). For a fixed value of l , we identify the critical volume fraction at which percolation occurs as the value where $\mathbb{P} \approx 50\%$.⁴⁷ The natural first choice is to probe the percolation threshold for $l = 4.8r_f$ corresponding to two times the radius of the effective fillers estimated from the local density analysis. This leads to percolation at a nanofiller volume fraction that is reasonably close to (but slightly larger than) that denoting the onset of reinforcement, as shown in Figure 4. We find that the onset of percolation and the onset of reinforcement occur at the same nanofiller volume fraction for $l \sim 6.4r_f$, which would correspond to a shell thickness of $\delta \sim 2.2r_f$, close to the value obtained from the local density

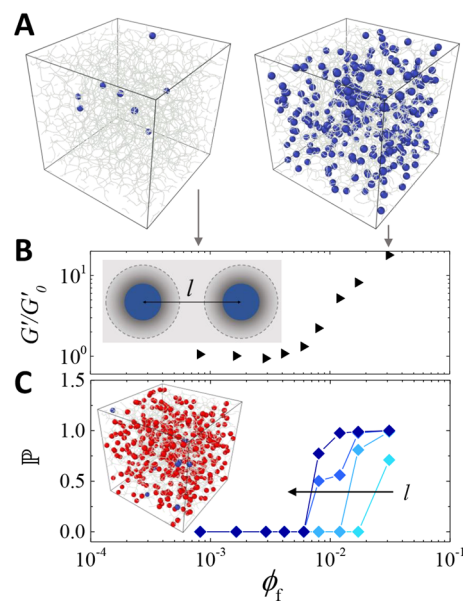


Figure 4. Percolation of effective fillers, composed of the nanofillers and their reinforced shells. (A) Snapshots of composites with the lowest (left) and highest volume fraction of nanofillers ϕ_f considered. The nanofillers are colored blue, the gel network is colored gray. (B) Normalized storage modulus versus ϕ_f and definition of the connectivity distance l . (C) Percolation probability \mathbb{P} of effective fillers versus ϕ_f for connectivity distances $l = 4.8r_f, 5.6r_f, 6.4r_f$ and $7.2r_f$ (right to left). In the snapshot, the particles in red belong to a single percolating cluster for $\phi_f = 0.03$ and $2\delta = 4.8r_f$.

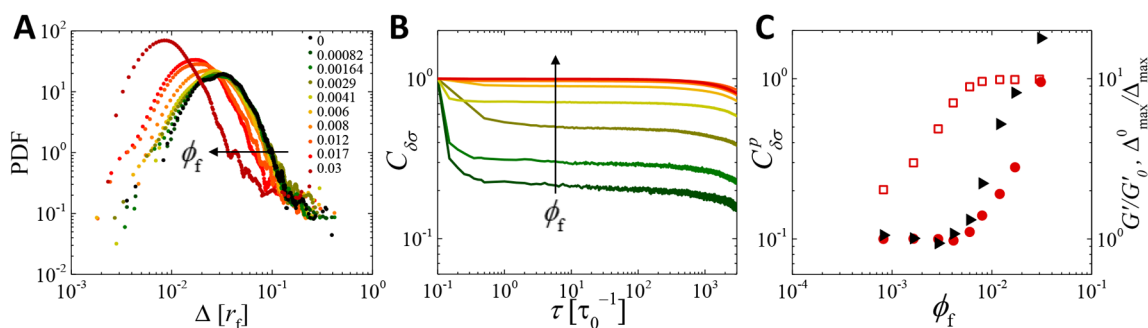


Figure 5. Reduced gel displacements and enhanced stress coupling beyond the onset of percolation in MD simulations. (A) Probability distribution functions (PDF) of gel displacements Δ for different ϕ_f . (B) Autocorrelation function of stress fluctuations versus delay time τ for different ϕ_f . (C) The onset of reinforcement of the normalized storage modulus G'/G'_0 (\blacktriangleright) coincides with the onset of increase of the inverse peak gel displacement, $\Delta_{\max}^0/\Delta_{\max}$ (\bullet) and the plateau of the stress fluctuation autocorrelation $C_{\delta\sigma}^p$ reaching a value of unity (\square).

measurement. This analysis supports the hypothesis that reinforcement is linked to the percolation of the densified regions induced by the nanofillers throughout the composite material.

To probe the effect of this percolated structure on the dynamics of the composite, we measure the microscopic displacements of the particles that form the model gel matrix. We obtain the displacement distributions from the long-time microscopic dynamics due to thermal fluctuations (see the [Numerical Methods](#)). The thermal fluctuations are weak enough to not induce significant changes in the gel topology via breaking and reforming the gel network within the time window of the simulations, but strong enough to govern the microscopic motion of the gel components.⁴⁸ We measure the gel displacement $\Delta_i = \|\mathbf{r}_i(t_0 + t_w) - \mathbf{r}_i(t_0)\|$ from the particle position $\mathbf{r}_i(t) \equiv (x(t), y(t), z(t))$ of particle i at time t , where x , y , and z represent the Cartesian coordinates. t_0 represents the initial time, and t_w the waiting time for the measurements.

The probability distribution function (PDF) of the gel particle displacements Δ is identical with that of the gel network without nanofillers for ϕ_f below the onset of reinforcement, as shown in [Figure 5A](#). For ϕ_f beyond the onset of reinforcement, however, the PDF shifts toward increasingly smaller displacements. The displacement corresponding to the maximum of the distribution, Δ_{\max} , normalized by the maximum of the displacement distribution of the gel without nanofillers, Δ_{\max}^0 , mirrors the ϕ_f -dependence of the storage modulus, as shown in [Figure 5C](#). A localization of the microscopic dynamics with an increasing amount of fillers has also been observed in un-cross-linked polymer matrices filled with nanoparticles.^{18,20,21} Here, it suggests that the presence of a percolating network of effective fillers connected through the gel matrix is associated with a reduction of the soft modes of the gel, which leads to an effective stiffening of the gel matrix.

To investigate how the percolating network affects the stress transmission throughout the composite material and its stiffening, we measure the microscopic stress fluctuations in the simulations and extract their time correlations. Variations in the time correlations of stress fluctuations provide information about possible changes in the mechanical coupling between the nanofillers and the gel, which should be enhanced upon percolation of the effective fillers. To facilitate the measurements, we slightly perturb the gel network by randomly removing bonds, as described in the literature⁴⁸ (see [Numerical Methods](#)). While the use of the bond removal

dynamics allows us to efficiently sample stress fluctuations over the simulation time window, we have verified that the bond removal rate is low enough not to change the network topology and its mechanical properties significantly and that the intrinsic dynamics of the gel dominated by thermal fluctuations and solvent damping are not significantly modified. We compute the instantaneous normal stresses as $\sigma_n = \frac{1}{3}(\sigma_{xx} + \sigma_{yy} + \sigma_{zz})$, where each stress component σ_{ij} is calculated from the virial expression (see [Numerical Methods](#)). From the time series of the fluctuating microscopic normal stress $\sigma_n(\tau)$ (reported in the [Supporting Information](#)), we compute the time autocorrelation function of the stress fluctuations $\delta\sigma$:

$$C_{\delta\sigma}(\tau) = \frac{\frac{1}{k-k_\tau+1} \sum_{t=0}^{t_k-\tau} (\sigma_n(t+\tau) - \langle\sigma_n\rangle)(\sigma_n(t) - \langle\sigma_n\rangle)}{\frac{1}{k_\tau+1} \sum_{t=0}^{\tau} (\sigma_n(t) - \langle\sigma_n\rangle)(\sigma_n(t) - \langle\sigma_n\rangle)} \quad (1)$$

where k is the total number of data points in the time series ($t_0, t_1, \dots, \tau, \dots, t_k$), k_τ represents the number of data points in (t_0, t_1, \dots, τ), and $\delta\sigma = \sigma_n - \langle\sigma_n\rangle$ is computed at delay time τ .⁴⁸ If the microscopic stresses fluctuate independently over time across the gel matrix, then we expect the correlation function to gradually decay to zero. If long-range spatial correlations are present in the gel, however, the temporal autocorrelation function does not fully decay over a large time window. For all gels with nanofiller volume fraction below the onset of reinforcement, the stress fluctuations time autocorrelation function initially decays, suggesting that the thermal fluctuations enable the internal normal stresses to partially decouple, as shown in [Figure 5B](#). $C_{\delta\sigma}(\tau)$ then reaches a plateau, indicating that the stresses are correlated in space and time, as expected in rigid samples. With increasing nanofiller volume fraction, the height of the plateau increases and reaches $C_{\delta\sigma}^p \approx 1$ for $\phi_f > 0.006$. The microscopic stresses throughout the network remain increasingly coupled over time, consistent with the stiffening of the material.

We find that the nanofiller volume fraction beyond which the stress fluctuations remain fully correlated corresponds to the volume fraction denoting the onset of reinforcement of the storage modulus and the percolation threshold estimated in [Figure 4C](#), as highlighted in [Figure 5C](#). An increase in the nanofiller content thus leads to an exceedingly stronger coupling of the stress fluctuations across the composite

material and to a full coupling as the effective fillers percolate. It is interesting to note that a similar increase in the stress fluctuation autocorrelation function has been observed in polymer melts with increasing nanofiller volume fraction²⁰ and in biopolymer networks with embedded stiff cells.^{29,30}

The physical mechanism for the reinforcement in our composites relies on a volume of reinforced gel around the nanofillers, which forms due to the attraction between the gel and the nanofillers. The presence of a bound layer of polymer around nanofillers that are attractive with the surrounding matrix has been established in various experiments.^{46,49} In polymer melts containing spherical nanofillers, the bound polymer chains bridge the nanofillers, which form a percolating network at high enough volume fraction reinforcing the composite.^{25,26} In our systems, the nanofillers also interact attractively with the matrix in which they are embedded, but the matrix is a self-assembled network rather than a polymer melt. The rigid hydrogel network surrounding the nanofillers guarantees long-range stress propagation and leads to significant reinforcement even at a low nanofiller volume fraction.

When varying the filler–matrix attraction strength in the simulations, we note a larger variation in reinforcement strength than that in experiments, which could be attributed to the relatively limited net variation of the attractive interactions between nanofillers and hydrogel matrices across the experimental systems. Systematically quantifying this effect, however, is beyond the scope of this study. Here, we focus on understanding the microscopic origin of the reinforcement. The reinforcement resulting from the general mechanism we identify does not require sophisticated engineering of the filler–matrix interactions, since a wide range of nonspecific attractive interactions can lead to a shell formation. It is thus distinct from the idea, proposed in other systems, that the nanofillers may act as additional cross-linking sites.^{12–16} Indeed, the weak dependence of the reinforcement on nanofiller size in our experiments suggests that the nanofillers are here not acting as cross-linkers. Additional evidence is provided by the magnitude of the shell thickness, which is on the order of the nanofiller radius rather than being strictly localized to the nanofiller surface. This highlights that beyond the addition of filler–gel bonds at the nanofiller surface, it is the local densification that is important in our mechanism, consistent with the finding that the volume of the nanofillers (and not their surface area) is a governing parameter for the reinforcement. That the reinforcement does not scale with the total nanofiller surface area further suggests that it is not limited by the number of binding sites per nanofiller. This emphasizes the role of effective filler percolation in the reinforcement. In the simulations we have further directly verified that the reinforcement induced by the nanofillers is not equivalent to that obtained by adding a similar number of additional cross-links in the gel matrix. Although the local densification around the nanofillers can still induce additional cross-linking in the gel matrix, we here provide a deeper physical insight into the mechanism of mechanical reinforcement through constraining the gel microscopic dynamics and enhancing the stress transmission. The same mechanism could apply to a range of attractive filler–gel systems that exhibit reinforcement at low volume fractions.^{38,39} The mechanism we identify here thus complements strategies based on multifunctional cross-links and provides the opportunity to reach a

strong reinforcement without precisely tuning the nanofiller surface chemistry to match that of the polymer.

CONCLUSIONS

Our combined experimental and computational study demonstrates the strong reinforcement at a low nanofiller volume fraction in hydrogels with attractive filler–matrix interactions. We provide a general mechanism by which the nanofillers induce an increase of the hydrogel storage modulus in systems of varying nanofiller size, chemistry, and concentration of the gel matrix. The attraction between the two components causes local densification of the hydrogel in the vicinity of the nanofillers, leading to the formation of a shell that is stiffer than the hydrogel network without nanofillers. With increasing volume fraction, the effective fillers, composed of the nanofillers and their surrounding reinforced shells, form a percolating network that restricts the microscopic fluctuations of the gel matrix, coupling the stress propagation throughout the system and ultimately inducing global stiffening of the composite. Key elements for strong reinforcement are the attractive interactions between the two components and the capability of the gel to reorganize itself around the nanofillers. As these features are largely independent of the molecular details of the components, this mechanism can guide the design of reinforced gels to create materials that exhibit both increased mechanical properties and tailored functionalities, including electrical conductivity or transparency inherent to the selected components.

MATERIALS AND METHODS

Experimental Section. *Preparation of Nanofiller-Hydrogel Composites.* We embed carboxylate-modified polystyrene nanoparticles (Magsphere) of radius r_f ranging between 20 and 500 nm into hydrogels composed of agarose, gelatin, or polyacrylamide. We add the particles to the aqueous solution at a volume fraction ϕ_f varying between 10⁻³% v/v and 10% v/v, so that the hydrogel forms in the presence of the nanoparticles. Agarose (A9539, Sigma-Aldrich) at a concentration ranging between 0.5 and 4 wt % is dissolved in deionized water with 0.01 M phosphate buffered saline (Corning, Cell Culture PBS (1X)) in the presence of polystyrene nanoparticles under stirring at 80 °C for 20 min. Gelatin type B (G9391, Sigma-Aldrich) is dissolved in deionized water at 6 wt % in the presence of polystyrene nanoparticles under stirring at 60 °C for 20 min. 7.1 wt % acrylamide, 1.7 wt % bis(acrylamide), and 0.17 wt % initiator VAZO56 (2, 2'-azobis(2-methylpropionamide) dihydrochloride) (Sigma-Aldrich) are dissolved in deionized water in the presence of polystyrene nanoparticles under stirring at 25 °C.

Rheological Measurements. The sample is loaded in a liquid state in a parallel-plate geometry (diameter $d = 40$ mm, initial gap height $h_0 = 500 \mu\text{m}$) connected to a stress-controlled rheometer (AR-G2, TA Instruments). Heated agarose and gelatin samples are placed on a preheated geometry, and the gelation is induced by decreasing the temperature at 5 °C/min from 80 to 25 °C for agarose samples and from 60 to 10 °C for gelatin samples. The final ramp temperature is ≈ 12 °C lower than the gelation temperature of the agarose and gelatin gels. Polyacrylamide gels are formed by a sudden temperature increase from 25 to 60 °C. The initiator is active beyond 56 °C. The rheological properties are monitored at the final ramp or quench temperature under small amplitude oscillations at strain amplitude $\gamma_0 = 1\%$ and frequency $f = 1$ Hz (see the Supporting Information). Our protocol ensures that the gels are not subjected to external stresses prior to the rheological measurements and thus minimizes any possible mechanical history. Moreover, we verified that the values of the plateau moduli are independent of the temperature ramp and quench rate. We use a zero normal force protocol to compensate for a possible contraction of the sample during the gelation.⁵⁰ The normal

force is maintained at $F_N = 0$ N, while the gap height h varies to compensate for changes in the sample height; h decreases by, at most, 10% during the gelation. The viscoelastic properties reach a steady state 5 to 15 min after the final ramp or quench temperature is reached, characterized by quasi-constant values of the storage modulus G' and the loss modulus G'' . We report G' and G'' 10 min into the steady state. Data are plotted as symbols and error bars: symbols refer to the median value and error bars refer to the minimum and maximum values around the median over a 10 min period in steady state.

Numerical Methods. Numerical Model. We use a particle-based model to simulate the gel-filler composite. In our model, for N gel particles and N_f nanofiller particles with position vectors $\{\mathbf{r}_1, \dots, \mathbf{r}_N, \mathbf{r}_{N+1}, \dots, \mathbf{r}_{N+N_f}\}$, the total interaction energy of the composite system is

$$U(\mathbf{r}_1, \dots, \mathbf{r}_{N+N_f}) = U^{\text{gel}} + \sum_{i>j}^{N_f} u_2^{\text{filler}}(\mathbf{r}_{ij}) + \sum_{i>j}^{N+N_f} u_2^{\text{filler-gel}}(\mathbf{r}_{ij}) \quad (2)$$

where the vector separation $\mathbf{r}_{ij} = \mathbf{r}_j - \mathbf{r}_i$ is measured in units of gel particle diameter d . U^{gel} is the potential energy for the gel matrix, which consists of a short-range attraction u_2^{gel} between the gel particles (the depth of the attractive well ϵ defines the energy unit in the simulations), and an angular term u_3^{gel} that provides bending rigidity between the bonds and controls the local connectivity. The details of each term are described in previous work^{48,51–55} and in the **Supporting Information**. The nanofillers interact via u_2^{filler} , a purely repulsive truncated and shifted Lennard-Jones potential in the form of the Weeks–Chandler–Anderson (WCA) potential:⁵⁶

$$u_2^{\text{filler}}(\mathbf{r}) = \begin{cases} 4\epsilon \left[\left(\frac{d_f}{r} \right)^{12} - \left(\frac{d_f}{r} \right)^6 \right] + \epsilon, & \text{for } r \leq 2^{1/6} d_f \\ 0, & \text{otherwise} \end{cases} \quad (3)$$

where d_f is the diameter of the nanofiller. This expression ensures that both the potential and force smoothly go to zero at the cutoff ($2^{1/6} d_f$). We have studied this model for nanofiller sizes between $d_f = 1d$ and $d_f = 2d$. The results shown in the paper refer to $d_f = 1.6d$, which is representative of the behavior obtained for $d_f > d$, for filler-gel interactions that can be either repulsive or attractive. In the case of repulsive filler-gel interactions, the interaction potential $u_2^{\text{filler-gel}}$ has the same form as in eq 3, where the diameter d_f is now replaced by an effective diameter $(d_f + d)/2$. For attractive filler-gel interactions, the sticky fillers interact with the gel through a potential $u_2^{\text{filler-gel}}$, which has the same functional form of u_2^{gel} with an effective diameter $(d_f + d)/2$.

All data have been obtained with gel matrices made of $N = 16000$ gel particles. The number of nanofiller particles varies between $N_f = 32$ and 10677.

Initial Configuration. The MD simulations are performed using the open-source LAMMPS software⁵⁷ appropriately modified to incorporate the interaction potential (eq 2). The initial gel structures are prepared via Molecular Dynamics (MD) simulations with periodic boundaries in three dimensions. The gel spontaneously self-assembles by slowly cooling the gel particles and successively bringing the particle assembly to a local minimum of the collective potential energy using dissipative dynamics, following the protocol described in the literature.^{48,51–55,58} To generate the composite structures, we use two different protocols, which are denoted P_1 and P_2 . In protocol P_1 , we insert N_f nanofillers of diameter d_f randomly into available empty spaces of the already self-assembled gel network before switching on the gel-filler interaction. In the P_2 protocol, the gel network is formed in the presence of nanofillers. All data discussed here refer to protocol P_1 , whereas results obtained with P_2 are provided for comparison in the **Supporting Information**.

In protocol P_1 , the stresses created by the introduction of new interactions due to the nanofillers are relaxed by using the dissipative dynamics:

$$m \frac{d^2 \mathbf{r}_i}{dt^2} = -\nabla_{\mathbf{r}_i} U - \zeta \frac{d\mathbf{r}_i}{dt} \quad (4)$$

where m is the mass of each particle and ζ represents the drag coefficient of the surrounding solvent. In protocol P_2 , instead, we initially place gel and filler nanoparticles randomly in a cubic simulation box at $k_B T/\epsilon = 0.5$, then reduce the ratio to $k_B T/\epsilon = 0.05$ in 10^7 MD steps with a Nose–Hoover thermostat.⁵⁹ At this point, a gel network is formed in the presence of nanofillers, and we further equilibrate the network for another 10^7 MD steps at $k_B T/\epsilon = 0.05$. The energy minimization is carried out using the dissipative dynamics reported in eq 4.

To minimize aging effects and the evolution of the number of filler-gel contacts, these configurations prepared from both P_1 and P_2 close to a local energy minimum, are then equilibrated at $k_B T/\epsilon = 10^{-4}$ for 2×10^7 MD steps, to study the dynamics and mechanics of the composite in the presence of thermal fluctuations. Different amounts of thermal fluctuations are introduced using a Langevin dynamics

$$m \frac{d^2 \mathbf{r}_i}{dt^2} = -\nabla_{\mathbf{r}_i} U - \zeta \frac{d\mathbf{r}_i}{dt} + F_i^r(t) \quad (5)$$

where $F_i^r(t)$ is a random force related to the drag coefficient ζ and to the temperature T : $\langle F_i^r(t) F_j^r(t') \rangle = 2\zeta k_B T \delta_{ij} \delta(t - t')$. We use MD reduced units, where the diameter d of the gel particle is the unit of distance, ϵ the unit of energy, m the unit of mass, and $\tau_0 = \sqrt{md^2/\epsilon}$ the unit of time. We use a time step $\Delta t = 0.005 \tau_0$ for integrating the equations of motion, and the drag coefficient $\zeta = 10m/\tau_0$ ensures that all dynamics are overdamped. We obtain a gel network at a volume fraction $\phi = 0.1$ by fixing the simulation box $L = 43.76d$, where the volume fraction ϕ is estimated considering the particles as spheres of diameter d . The simulations cover a range of nanofiller volume fractions $\phi_f \sim N_f \pi d_f^3 / 6L^3 \sim 0.00082 - 0.273$. For attractive nanofillers, the strength of interaction between gel and filler nanoparticles is varied by modifying the depth of the interaction potential through the parameter A in

$$u_2^{\text{filler-gel}}(\mathbf{r}) = A \left[\left(\frac{d + d_f}{2r} \right)^{18} - \left(\frac{d + d_f}{2r} \right)^6 \right]$$

Gel Density. The gel density is computed based on the number density of gel particles in a given volume. For the pure gel density, this volume is the simulation box, and for the local densification measurements, the volume is that of the layer surrounding the nanofillers. We obtain the probability distribution functions, which we fit using a Gaussian distribution. We report the mean and standard deviation of the Gaussian fit in **Figure 3**.

Microscopic Dynamics and Displacement Distributions. The magnitude of gel particle displacement is computed as $\Delta_i = \|\mathbf{r}_i(t_0 + t_w) - \mathbf{r}_i(t_0)\|$ from the position of particle i at time t $\mathbf{r}_i(t) \equiv (x(t), y(t), z(t))$, where x , y , and z represent the Cartesian coordinates. The initial time t_0 is chosen in the vicinity of the plateau in the particle mean-squared displacement (see the **Supporting Information**). We use the initial time $t_0 = 10^4 \tau_0$ and waiting time $t_w = 10^4 \tau_0$.

Stress Fluctuations and Time Autocorrelation Functions. The stresses are computed from the interaction part of the global stress tensor using the standard virial equation⁶⁰ while neglecting other contributions (kinetic and viscous terms):

$$\sigma_{\alpha\beta} = \frac{1}{V} \sum_{i=1}^N \frac{\partial U}{\partial r_i^\alpha} r_i^\beta \quad (6)$$

where α and β denote the Cartesian components $\{x, y, z\}$ and V represents the volume of the simulation box. The normal stress is computed as $\sigma_n = \frac{1}{3}(\sigma_{xx} + \sigma_{yy} + \sigma_{zz})$. To induce the normal stress fluctuations $\delta\sigma = \sigma_n - \langle \sigma_n \rangle$, we use a constant rate of bond removal that is $0.02 \tau_0^{-1}$,⁴⁸ which guarantees a negligible change in the network topology since only $\sim 1\%$ of the total bonds are removed over the duration of the simulations (2×10^8 MD steps). We monitor the

evolution of the normal stresses using the Langevin dynamics (eq 5) with the same amount of thermal fluctuations $k_B T/\epsilon = 10^{-4}$ used in the calculations of microscopic displacements (see the Supporting Information).

Computational Rheology. The linear viscoelastic spectrum for composites with different volume fractions of nanofillers is obtained by imposing an optimally windowed chirp (OWCh) signal containing multiple frequencies.⁶¹ This method has better accuracy and efficiency than traditional discrete frequency sweep simulations. The OWCh signal $\gamma(t)$ is used as an input in the xy -plane through

$$m \frac{d^2 \mathbf{r}_i}{dt^2} = -\nabla_{\mathbf{r}_i} U - \zeta \left(\frac{d\mathbf{r}_i}{dt} - \dot{\gamma}(t) \gamma_i \mathbf{e}_x \right) + \mathbf{F}_r^i(t) \quad (7)$$

updating the Lees–Edwards boundary conditions at every time step. Here \mathbf{e}_x denotes the unit vector in the x -direction. The thermal fluctuations are kept at $k_B T/\epsilon = 10^{-4}$ and introduced through a random force $\mathbf{F}_r^i(t)$. Under applied deformation, we compute the instantaneous shear stress $\sigma_{xy}(t)$ by using eq 6. The complex viscoelastic modulus $G^*(\omega)$ is obtained from the Fourier transforms of the stress output $\tilde{\sigma}(\omega)$ and the strain input $\tilde{\gamma}(\omega)$ signals as $G^*(\omega) = \tilde{\sigma}(\omega)/\tilde{\gamma}(\omega)$ from which we compute the storage modulus G' and the loss modulus G'' defined as the real and imaginary part of G^* , respectively. All the systems studied exhibit a finite storage modulus G'_p at low frequencies, as shown in the Supporting Information. For simplicity, we represent G'_p as G' and report it as a function of the nanofiller volume fraction for the two protocols P_1 and P_2 in the Supporting Information. The data shown in the manuscript refer to P_1 .

ASSOCIATED CONTENT

Supporting Information

The Supporting Information is available free of charge at <https://pubs.acs.org/doi/10.1021/acsnano.3c00716>.

- (1) Mesh size of agarose gels (Table S1);
- (2) Fit parameters of the two-step reinforcement model (Table S2);
- (3) Microscopic characterization of the nanofillers in the composite (Figure S1);
- (4) Adaptation of the Guth–Gold model (Figure S2);
- (5) Description of the gel model in MD simulations;
- (6) Description of the gel preparation in MD simulations;
- (7) Normal stress fluctuations obtained in simulations (Figure S3);
- (8) Linear viscoelastic properties of hydrogels during and after gelation (Figure S4);
- (9) Mean-squared displacements obtained in simulations (Figure S5);
- (10) Linear viscoelastic properties of gels obtained in simulations (Figure S6);
- (11) Reinforcement of gels prepared with different protocols in MD simulations (Figure S7) (PDF)

AUTHOR INFORMATION

Corresponding Authors

Ippolyti Dellatolas – Department of Mechanical Engineering, Massachusetts Institute of Technology, Cambridge, Massachusetts 02139, United States; orcid.org/0000-0002-3431-8450; Email: ippolyti@mit.edu

Irmgard Bischofberger – Department of Mechanical Engineering, Massachusetts Institute of Technology, Cambridge, Massachusetts 02139, United States; orcid.org/0000-0002-7067-6626; Email: irmgard@mit.edu

Authors

Minaspi Bantawa – Department of Physics and Institute for Soft Matter Synthesis and Metrology, Georgetown University, Washington, D.C. 20057, United States

Brian Damerou – Department of Physics and Institute for Soft Matter Synthesis and Metrology, Georgetown University, Washington, D.C. 20057, United States

Ming Guo – Department of Mechanical Engineering, Massachusetts Institute of Technology, Cambridge, Massachusetts 02139, United States; orcid.org/0000-0002-0016-4158

Thibaut Divoux – ENSL, CNRS, Laboratoire de Physique, F-69342 Lyon, France; MultiScale Material Science for Energy and Environment, UMI 3466, CNRS-MIT, Massachusetts Institute of Technology, Cambridge, Massachusetts 02139, United States; orcid.org/0000-0002-6777-5084

Emanuela Del Gado – Department of Physics and Institute for Soft Matter Synthesis and Metrology, Georgetown University, Washington, D.C. 20057, United States; orcid.org/0000-0002-8340-0290

Complete contact information is available at:

<https://pubs.acs.org/doi/10.1021/acsnano.3c00716>

Author Contributions

*I.D. and M.B. contributed equally. I.D., M.B., T.D., E.D.G., and I.B. designed the research; I.D. performed the experiments; M.B. and B.D. conducted the simulations; I.D., M.B., M.G., T.D., E.D.G., and I.B. analyzed the experimental and numerical data; I.D., M.B., T.D., E.D.G., and I.B. wrote the paper.

Funding

I.D. and I.B. acknowledge support from the MIT-France program, from the MIT International Science and Technology Initiative, and from the Fondation de l'École des Mines de Paris. I.D. acknowledges support from a MathWorks Fellowship and a MIT George and Marie Vergottis Fellowship. T.D. acknowledges support from the National Science Foundation under Grant No. NSF PHY 17–48958 through the KITP program on the Physics of Dense Suspensions. M.B. and E.D. acknowledge support from the National Science Foundation (NSF DMR-2026842). B.D. acknowledges a Hichwa Fellowship from the Department of Physics at Georgetown University.

Notes

The authors declare no competing financial interest.

ACKNOWLEDGMENTS

The authors thank Guilhem Baeza, Fei Deng, Urs Gasser, Ruipeng Li, and Yun Liu for helpful discussions.

REFERENCES

- (1) Yoshida, R. Design of Functional Polymer Gels and Their Application to Biomimetic Materials. *Curr. Org. Chem.* **2005**, *9*, 1617–1641.
- (2) Liang, Y.; He, J.; Guo, B. Functional Hydrogels as Wound Dressing to Enhance Wound Healing. *ACS Nano* **2021**, *15*, 12687–12722.
- (3) Li, J.; Mooney, D. J. Designing hydrogels for controlled drug delivery. *Nat. Rev. Mater.* **2016**, *1*, 16071.
- (4) Thakur, S.; Thakur, V. K.; Arotiba, O. A. History, Classification, Properties and Application of Hydrogels: An Overview. *Hydrogels: Recent Advances*. Springer **2018**, 29–50.
- (5) Xavier, J. R.; Thakur, T.; Desai, P.; Jaiswal, M. K.; Sears, N.; Cosgriff-Hernandez, E.; Kaunas, R.; Gaharwar, A. K. Bioactive Nanoengineered Hydrogels for Bone Tissue Engineering: A Growth-Factor-Free Approach. *ACS Nano* **2015**, *9*, 3109–3118.

- (6) Ayyub, O. B.; Kofinas, P. Enzyme Induced Stiffening of Nanoparticle–Hydrogel Composites with Structural Color. *ACS Nano* **2015**, *9*, 8004–8011.
- (7) Calvert, P. Hydrogels for Soft Machines. *Adv. Mater.* **2009**, *21*, 743–756.
- (8) Zhao, X.; Chen, X.; Yuk, H.; Lin, S.; Liu, X.; Parada, G. Soft Materials by Design: Unconventional Polymer Networks Give Extreme Properties. *Chem. Rev.* **2021**, *121*, 4309–4372.
- (9) Holten-Andersen, N.; Harrington, M. J.; Birkedal, H.; Lee, B. P.; Messersmith, P. B.; Lee, K. C.; Waite, J. H. pH-induced metal-ligand cross-links inspired by mussel yield self-healing polymer networks with near-covalent elastic moduli. *Proc. Natl. Acad. Sci. U.S.A.* **2011**, *108*, 2651–2655.
- (10) Tsukeshiba, H.; Huang, M.; Na, Y.; Kurokawa, T.; Kuwabara, R.; Tanaka, Y.; Furukawa, H.; Osada, Y.; Gong, J. P. Effect of Polymer Entanglement on the Toughening of Double Network Hydrogels. *J. Phys. Chem. B* **2005**, *109*, 16304–16309.
- (11) Mao, Y.; Lin, S.; Zhao, X.; Anand, L. A large deformation viscoelastic model for double-network hydrogels. *J. Mech. Phys. Solids* **2017**, *100*, 103–130.
- (12) Haraguchi, K.; Takehisa, T. Nanocomposite hydrogels: a unique organic–inorganic network structure with extraordinary mechanical, optical, and swelling/de-swelling properties. *Adv. Mater.* **2002**, *14*, 1120–1124.
- (13) Haraguchi, K. Nanocomposite hydrogels. *Curr. Opin. Solid State Mater. Sci.* **2007**, *11*, 47–54.
- (14) Wu, Y.; Zhou, Z.; Fan, Q.; Chen, L.; Zhu, M. Facile in-situ fabrication of novel organic nanoparticle hydrogels with excellent mechanical properties. *J. Mater. Chem.* **2009**, *19*, 7340–7346.
- (15) Gu, S.; Duan, L.; Ren, X.; Gao, G. H. Robust, tough and anti-fatigue cationic latex composite hydrogels based on dual physically cross-linked networks. *J. Colloid Interface Sci.* **2017**, *492*, 119–126.
- (16) Liu, L.; Lv, G.; Ren, X.; Li, X.; Wang, T.; Dong, J.; Wang, Z.; Wu, G. Effect of size of latex particles on the mechanical properties of hydrogels reinforced by latex particles. *RSC Adv.* **2019**, *9*, 14701–14707.
- (17) Jaiswal, M. K.; Xavier, J. R.; Carrow, J. K.; Desai, P.; Alge, D.; Gaharwar, A. K. Mechanically Stiff Nanocomposite Hydrogels at Ultralow Nanoparticle Content. *ACS Nano* **2016**, *10*, 246–256.
- (18) Smith, G. D.; Bedrov, D.; Li, L.; Bytner, O. A molecular dynamics simulation study of the viscoelastic properties of polymer nanocomposites. *J. Chem. Phys.* **2002**, *117*, 9478–9489.
- (19) Papakonstantopoulos, G. J.; Doxastakis, M.; Nealey, P. F.; Barrat, J.-L.; de Pablo, J. J. Calculation of local mechanical properties of filled polymers. *Phys. Rev. E* **2007**, *75*, 031803.
- (20) Sen, S.; Thomin, J. D.; Kumar, S. K.; Koblinski, P. Molecular Underpinnings of the Mechanical Reinforcement in Polymer Nanocomposites. *Macromolecules* **2007**, *40*, 4059–4067.
- (21) Kalathi, J. T.; Yamamoto, U.; Schweizer, K. S.; Grest, G. S.; Kumar, S. K. Nanoparticle Diffusion in Polymer Nanocomposites. *Phys. Rev. Lett.* **2014**, *112*, 108301.
- (22) Pavlov, A. S.; Khalatur, P. G. Filler reinforcement in cross-linked elastomer nanocomposites: insights from fully atomistic molecular dynamics simulation. *Soft Matter* **2016**, *12*, 5402–5419.
- (23) Riggelman, R. A.; Toepferwein, G.; Papakonstantopoulos, G. J.; Barrat, J.-L.; de Pablo, J. J. Entanglement network in nanoparticle reinforced polymers. *J. Chem. Phys.* **2009**, *130*, 244903.
- (24) Karatrantos, A.; Clarke, N.; Composto, R. J.; Winey, K. I. Entanglements in polymer nanocomposites containing spherical nanoparticles. *Soft Matter* **2016**, *12*, 2567–2574.
- (25) Baeza, G. P.; Dessi, C.; Costanzo, S.; Zhao, D.; Gong, S.; Alegria, A.; Colby, R. H.; Rubinstein, M.; Vlassopoulos, D.; Kumar, S. K. Network dynamics in nanofilled polymers. *Nat. Commun.* **2016**, *7*, 1–6.
- (26) Chen, Q.; Gong, S.; Moll, J.; Zhao, D.; Kumar, S. K.; Colby, R. H. Mechanical Reinforcement of Polymer Nanocomposites from Percolation of a Nanoparticle Network. *ACS Macrolett.* **2015**, *4*, 398–402.
- (27) Puech, N.; Mora, S.; Phou, T.; Porte, G.; Jestin, J.; Oberdisse, J. Microemulsion nanocomposites: phase diagram, rheology and structure using a combined small angle neutron scattering and reverse Monte Carlo approach. *Soft Matter* **2010**, *6*, 5605–5614.
- (28) Baeza, G. P. The Reinforcement Effect in Well-Defined Segmented Copolymers: Counting the Topological Constraints at the Mesoscopic Scale. *Macromolecules* **2018**, *51*, 1957–1966.
- (29) van Oosten, A. S. G.; Chen, X.; Chin, L.; Cruz, K.; Patteson, A. E.; Pogoda, K.; Shenoy, V. B.; Janmey, P. A. Emergence of tissue-like mechanics from fibrous networks confined by close-packed cells. *Nature* **2019**, *573*, 96–101.
- (30) Shivers, J. L.; Feng, J.; van Oosten, A. S. G.; Levine, H.; Janmey, P. A.; MacKintosh, F. C. Compression stiffening of fibrous networks with stiff inclusions. *Proc. Natl. Acad. Sci. U.S.A.* **2020**, *117*, 21037–21044.
- (31) van Vliet, T. Rheological properties of filled gels. Influence of filler matrix interaction. *Colloid Polym. Sci.* **1988**, *266*, 518–524.
- (32) Richardson, R. K.; Robinson, G.; Ross-Murphy, S. B.; Todd, S. Mechanical spectroscopy of filled gelatin gels. *Polym. Bull.* **1981**, *4*, 541–546.
- (33) Genovese, D. B. Shear rheology of hard-sphere, dispersed, and aggregated suspensions, and filler-matrix composites. *Adv. Colloid Interface Sci.* **2012**, *171–172*, 1–16.
- (34) Brownsey, G. J.; Ellis, H. S.; Ridout, M. J.; Ring, S. G. Elasticity and Failure in Composite Gels. *J. Rheol.* **1987**, *31*, 635–649.
- (35) Guth, E. Theory of Filler Reinforcement. *J. Appl. Phys.* **1945**, *16*, 20–25.
- (36) Bergstrom, J. S.; Boyce, M. C. Mechanical Behavior of Particle Filled Elastomers. *Rubber Chem. Technol.* **1999**, *72*, 633–656.
- (37) Pal, R. Complex Shear Modulus of Concentrated Suspensions of Solid Spherical Particles. *J. Colloid Interface Sci.* **2002**, *245*, 171–177.
- (38) Lin, W. C.; Fan, W.; Marcellan, A.; Hourdet, D.; Creton, C. Large Strain and Fracture Properties of Poly(dimethylacrylamide)/Silica Hybrid Hydrogels. *Macromolecules* **2010**, *43*, 2554–2563.
- (39) Thevenot, C.; Khoukh, A.; Reynaud, S.; Desbrieres, J.; Grassl, B. Kinetic aspects, rheological properties and mechano-electrical effects of hydrogels composed of polyacrylamide and polystyrene nanoparticles. *Soft Matter* **2007**, *3*, 437–447.
- (40) Djabourov, M.; Nishinari, K.; Ross-Murphy, S. B. *Physical Gels from Biological and Synthetic Polymers*; Cambridge University Press, 2013.
- (41) Hsu, T. P.; Cohen, C. Observations on the structure of a polyacrylamide gel from electron micrographs. *Polymer* **1984**, *25*, 1419–1432.
- (42) Cosgrove, T.; Hone, J.; Howe, A. M.; Heenan, R. A Small-Angle Neutron Scattering Study of the Structure of Gelatin at the Surface of Polystyrene Latex Particles. *Langmuir* **1998**, *14*, 5376–5382.
- (43) Likos, C. N.; Vaynberg, K. A.; Lowen, H.; Wagner, N. J. Colloidal Stabilization by Adsorbed Gelatin. *Langmuir* **2000**, *16*, 4100–4108.
- (44) Tanaka, H.; Swerin, A.; Ödberg, L. Cleavage of Polymer Chains during Transfer of Cationic Polyacrylamide from Cellulose Fibers to Polystyrene Latex. *J. Colloid Interface Sci.* **1992**, *153*, 13–22.
- (45) Shubin, V.; Samoshina, Y.; Menshikova, A.; Evseeva, T. Adsorption of cationic polyelectrolyte onto a model carboxylic latex and the influence of adsorbed polycation on the charge regulation at the latex surface. *Colloid Polym. Sci.* **1997**, *275*, 655–660.
- (46) Deng, F.; Van Vliet, K. J. Prediction of elastic properties for polymer-particles nanocomposites exhibiting an interphase. *Nanotechnology* **2011**, *22*, 165703.
- (47) Stauffer, D.; Aharony, A. *Introduction to Percolation Theory*; CRC Press, 2018.
- (48) Bouzid, M.; Colombo, J.; Barbosa, L. V.; Del Gado, E. Elastically driven intermittent microscopic dynamics in soft solids. *Nat. Commun.* **2017**, *8*, 1–8.
- (49) Jouault, N.; Crawford, M. K.; Chi, C.; Smalley, R. J.; Wood, B.; Jestin, J.; Melnichenko, Y. B.; He, L.; Guise, W. E.; Kumar, S. K.

Polymer chain behavior in polymer nanocomposites with attractive interactions. *ACS Macrolett.* **2016**, *5*, 523–527.

(50) Mao, B.; Divoux, T.; Snabre, P. Normal force controlled rheology applied to agar gelation. *J. Rheol.* **2016**, *60*, 473–489.

(51) Colombo, J.; Del Gado, E. Stress localization, stiffening, and yielding in a model colloidal gel. *J. Rheol.* **2014**, *58*, 1089–1116.

(52) Bouzid, M.; Del Gado, E. Network Topology in Soft Gels: Hardening and Softening Materials. *Langmuir* **2018**, *34*, 773–781.

(53) Feng, D.; Notbohm, J.; Benjamin, A.; He, S.; Wang, M.; Ang, L. H.; Bantawa, M.; Bouzid, M.; Del Gado, E.; Krishnan, R.; Pollak, M. R. Disease-causing mutation in α -actinin-4 promotes podocyte detachment through maladaptation to periodic stretch. *Proc. Natl. Acad. Sci. U.S.A.* **2018**, *115*, 1517–1522.

(54) Vereroudakis, E.; Bantawa, M.; Lafleur, R. P. M.; Parisi, D.; Matsumoto, N. M.; Peeters, J. W.; Del Gado, E.; Meijer, E. W.; Vlassopoulos, D. Competitive Supramolecular Associations Mediate the Viscoelasticity of Binary Hydrogels. *ACS Cent. Sci.* **2020**, *6*, 1401–1411.

(55) Bantawa, M.; Fontaine-Seiler, W. A.; Olmsted, P. D.; Del Gado, E. Microscopic interactions and emerging elasticity in model soft particulate gels. *J. Phys.: Condens. Matter* **2021**, *33*, 414001.

(56) Weeks, J. D.; Chandler, D.; Andersen, H. C. Role of Repulsive Forces in Determining the Equilibrium Structure of Simple Liquids. *J. Chem. Phys.* **1971**, *54*, 5237–5247.

(57) Plimpton, S. Fast Parallel Algorithms for Short-Range Molecular Dynamics. *J. Comput. Phys.* **1995**, *117*, 1–19.

(58) Colombo, J.; Widmer-Cooper, A.; Del Gado, E. Microscopic Picture of Cooperative Processes in Restructuring Gel Networks. *Phys. Rev. Lett.* **2013**, *110*, 198301.

(59) Todd, B. D.; Daivis, P. J. *Nonequilibrium Molecular Dynamics: Theory, Algorithms and Applications*; Cambridge University Press, 2017.

(60) Thompson, A. P.; Plimpton, S. J.; Mattson, W. General formulation of pressure and stress tensor for arbitrary many-body interaction potentials under periodic boundary conditions. *J. Chem. Phys.* **2009**, *131*, 154107.

(61) Bouzid, M.; Keshavarz, B.; Geri, M.; Divoux, T.; Del Gado, E.; McKinley, G. H. Computing the linear viscoelastic properties of soft gels using an optimally windowed chirp protocol. *J. Rheol.* **2018**, *62*, 1037–1050.